A Rigorous SAR Epipolar Geometry Modeling and Application to 3D Target Reconstruction

Dong Li, *Student Member*, *IEEE* and Yunhua Zhang, *Member*, *IEEE*

ABSTRACT

A rigorous modeling of SAR epipolar geometry is developed from a concise SAR imaging model proposed in the paper. The imaging model and epipolar model not only geometrically unifies the SAR imaging and the optical camera imaging, but also motivates a 3D target reconstruction which is theoretically validated to be consistent with the radargrammetry and experimentally demonstrated to be accurate.

Key Words: Epipolar geometry, imaging model, synthetic aperture radar (SAR), 3D target reconstruction.

I. INTRODUCTION

WHEN a spatially three-dimensional (3D) point is viewed by two sensors located at two positions, there is always a geometrical constraint between the two imaged pixels of the point [1-2]. This pixel relation is termed as the epipolar geometry of the stereo, which is also named the image geometrical warp function because it maps a pixel position in the first image into a different pixel position in the second image and forms the so-called image geometrical warp. The epipolar geometry of optical camera has been extensively studied in the field of computer vision, where the fundamental matrix and homography are the two widely-used descriptions of epipolar geometry when the pinhole imaging is considered. The existing researches on the modeling of epipolar geometry for synthetic aperture radar (SAR) mainly appear in SAR image registration because its task is to compensate the geometrical warp, wherein the epipolar geometry is often approximated as a low-order polynomial [3-5], such as the affine transformation [4], the similarity transformation [6], the scaling transformation [7], the skew transformation [8], as well as the second- and third-order polynomials [9-10]. The polynomials can not reflect the distortion sources during SAR image formation and also can not correct for the terrain relief distortions [11], thus they are only restricted to the

weakly distorted images from gently topographic area with short spatial baseline. Some researches on SAR interferometry (InSAR) and radargrammetry [5], [12], [13] have investigated the rough topography-induced geometrical warp, the obtained epipolar models, however, mainly focus on the warp of image translations because radargrammetry and InSAR usually adopt parallel tracks so as to control the image decorrelation [13]. Few researches have been carried out for the rigorous epipolar geometry of the general SAR stereo arrangement composed by any two SAR systems from any two geometries. However, we think research on this field is now very necessary because the available SAR data increase dramatically with the launch of many SAR systems recently, we are urgent to jointly process the multiple data for accurate perception of a scene, and the rigorous modeling of general epipolar geometry is the starting point of these applications.

The modeling of epipolar geometry in fact involves in the imaging model or orientation model of the sensor. SAR acquires image from the slant range, thus the 3D points which are imaged to the same pixel P_1 in the first image locate in a Doppler circle formed by the intersection of the range sphere and Doppler cone [2] [13]. These points are then imaged to a series of pixels on the second image through the slant projection of the second SAR sensor and compose the epipolar line of P_1, which is not a simple straight line anymore. Therefore, the description of SAR epipolar geometry with the fundamental matrix is inappropriate because it is only appropriate to the linear projection. SAR image usually covers a large ground scene with varied topography, thus the approximation of the 3D ground scene as a planar surface is inaccurate, which means the plane-induced homography is also inappropriate. In order to construct a rigorous description of SAR epipolar geometry, we seek to another idea in this paper to achieve it directly from the SAR imaging model. The imaging model maps a 3D point to its projective pixel, so we can relate the two imaged pixels of the point under two SAR projections by combining the two imaging relations. However, in order to guarantee a rigorous and analytical epipolar modeling, the imaging model should be accurate and concise. The existing SAR imaging models can be generally classified into two categories, i.e. the physical model and empirical model [11]. The physical model takes into account several aspects that influence the acquisition procedure based on the range-Doppler equations (RDEs) [13]. Theoretically, we can obtain an accurate SAR epipolar

model from the RDEs of the two SARs. However, the model may not be concise because of the complex nonlinearity of RDEs, which may impact the further application. The empirical model is used if the system parameter, imaging geometry, and physical model are unavailable. The polynomial and rational polynomial [11], [14] are the widely-used empirical models which are the extensions of homography and collinearity equations developed from the central projection, respectively. However, the equivalent projection center for slant range imaging is not fixed, which indicates SAR is a multi-central projection system or variable focus system, thus the empirical model is inaccurate.

In this paper, we develop a concise SAR imaging model in terms of several matrix transformations, based on which a rigorous modeling of epipolar geometry for general SAR stereo is deduced. It is shown that the obtained SAR imaging model and epipolar geometry can provide a geometrical unification of SAR imaging and camera imaging. The developed epipolar geometry is related not only to the system parameters and imaging geometries but also to the 3D target geometry. An epipolar geometry-based target reconstruction is further proposed and validated to be accurate.

The rest of the paper is arranged as follows. Section II presents the concise orientation model and epipolar geometry for SAR imaging, based on which a target reconstruction algorithm is developed in Section III, and Section IV finally concludes the paper.

II. Rigorous Modeling of SAR Epipolar Geometry

A. The Concise SAR Imaging Model

The rigorous modeling of SAR epipolar geometry requires the imaging model to be concise and accurate. To achieve this, we assume that the track of SAR platform is parallel to the ground plane, which indicates the influence from the curvature of earth and track is neglected, thus we mainly focus on the airborne SAR system. Nevertheless, we think it may also hold for the spaceborne SAR system if we can compensate those nonideal influences by using high precise platform-borne GPS and INS beforehand.

Here we consider a general SAR imaging geometry as shown in Fig. 1. The global coordinate system is

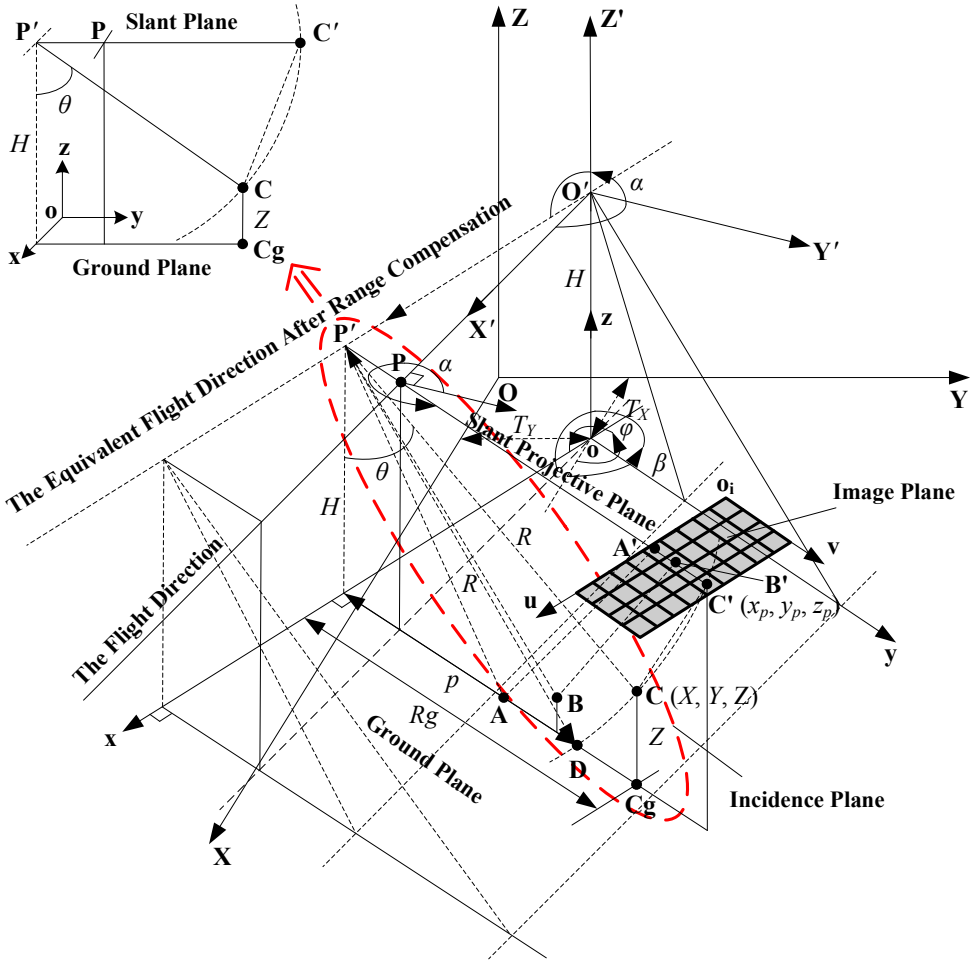

Fig. 1 The considered general SAR imaging geometry.

denoted as **O-XYZ**. The radar moves along a track of height H paralleling to the ground plane **XOY**. In order to describe the platform attitude, we establish a platform coordinate system **O'-X'Y'Z'**, where **O'** is located at (T_X, T_Y, H) in **O-XYZ** and represents the initial antenna phase center (APC), **X'** denotes the flight direction of the platform, **Z'** is parallel to **Z**, and **Y'** is the normal direction orthogonal to **X'** and **Z'**. If the flight direction **X'** is β deviated from **X**, where β refers to the angle that anti-clockwisely rotates **X** to **X'**, the transformation between **O'-X'Y'Z'** and **O-XYZ** can thus be expressed as:

$$\begin{pmatrix} X' \\ Y' \\ Z' \end{pmatrix} = \begin{pmatrix} \mathbf{R}_{\boldsymbol{\beta}} & \mathbf{0} \\ \mathbf{0}^T & 1 \end{pmatrix} \begin{pmatrix} X - T_X \\ Y - T_Y \\ Z - H \end{pmatrix} \quad \text{with} \quad \mathbf{R}_{\boldsymbol{\beta}} = \begin{pmatrix} \cos\beta & \sin\beta \\ -\sin\beta & \cos\beta \end{pmatrix} \tag{1}$$

where $\mathbf{0}$ is the zero vector of $[0, 0]^T$. We further consider a general imaging geometry that the antenna has a squint angle of α, where α refers to the angle that anti-clockwisely rotates **Y'** to the incidence plane. For

squint SAR, we should compensate the scattering to the zero Doppler centroid in either of the two image directions first. The azimuth compensation is equivalent to keeping the flight direction fixed while rotating the antenna boresight to be perpendicular to the flight direction. This equals to the side-looking imaging in view of the original flight track. The range compensation is equivalent to keeping the antenna boresight direction fixed while rotating the flight direction to be perpendicular to the boresight direction. So it equals to the side-looking imaging in view of the rotated track as shown in Fig. 1, which means the instantaneous APC **P** is equivalently transformed to **P'** with a rotation α. The azimuth compensation can be geometrically treated as a special case of range compensation with zero equivalent track rotation. Thus only the range compensation is considered in our model. Then the image is obtained by matched filtering the compensated scattering in range direction and aperture synthesizing in azimuth direction as the conventional side-looking Range-Doppler algorithm performs. After these, SAR imaging can be modeled as a geometrical projection from ground plane to slant plane as shown in Fig. 1. For the sake of convenience, we further define an imaging coordinate system **o-xyz**, where **o** is located at (T_X, T_Y, 0) in **O-XYZ**, **z** is parallel to **Z**, **y** is parallel to the ground projection of the antenna boresight, and **x** is orthogonal to **y** and **z**. The range compensation results in an anti-clockwise rotation of α from **X'** to **x**, thus the relation between **o-xyz** and **O'-X'Y'Z'** can be described as

$$\begin{pmatrix} x \\ y \\ z \end{pmatrix} = \begin{pmatrix} \mathbf{R}_{\boldsymbol{\alpha}} & \mathbf{0} \\ \mathbf{0}^T & 1 \end{pmatrix} \begin{pmatrix} X' \\ Y' \\ Z'+H \end{pmatrix} \quad \text{with} \quad \mathbf{R}_{\boldsymbol{\alpha}} = \begin{pmatrix} \cos\alpha & \sin\alpha \\ -\sin\alpha & \cos\alpha \end{pmatrix}. \tag{2}$$

We can then obtain the transformation from **O-XYZ** to **o-xyz** by combining (1) and (2)

$$\begin{pmatrix} x \\ y \\ z \end{pmatrix} = \begin{pmatrix} \mathbf{R} & \mathbf{0} \\ \mathbf{0}^T & 1 \end{pmatrix} \begin{pmatrix} X-T_X \\ Y-T_Y \\ Z \end{pmatrix} \quad \text{with} \quad \mathbf{R} = \mathbf{R}_{\boldsymbol{\alpha}}\mathbf{R}_{\boldsymbol{\beta}} = \begin{pmatrix} \cos\varphi & \sin\varphi \\ -\sin\varphi & \cos\varphi \end{pmatrix} \tag{3}$$

where φ denotes the anti-clockwise rotation from **X** to **x** and $\varphi = \alpha + \beta$.

Let **C** be a 3D point within the radar beam with coordinates of (X, Y, Z) and (x, y, z) in **O-XYZ** and **o-xyz**, respectively. After slant range projection, **C** is mapped to **C'** (x_p, y_p, z_p). From the projection geometry in

Fig. 1, we can easily obtain that

$$x_p = x,\ y_p = P'C' = P'C = y\sin^{-1}\theta,\ z_p = H. \tag{4}$$

where θ is the local radar incidence related to the position and height of **C**. Thus the relation between the slant projective plane and ground plane can be written as:

$$\begin{pmatrix} x_p \\ y_p \end{pmatrix} = \mathbf{M} \cdot \begin{pmatrix} x \\ y \end{pmatrix} \quad \text{with} \quad \mathbf{M} = \begin{pmatrix} 1 & 0 \\ 0 & \sin^{-1}\theta \end{pmatrix}. \tag{5}$$

The final SAR image is the sampling of the projective plane. Let's define an image coordinate system $\mathbf{o_i}$**-uv**, the relation between pixel (u, v) and projection (x_p, y_p, z_p) can then be expressed as:

$$\begin{pmatrix} u \\ v \end{pmatrix} = \begin{pmatrix} s_x & 0 \\ 0 & s_y \end{pmatrix} \begin{pmatrix} x_p - t_x \\ y_p - t_y \end{pmatrix} = \mathbf{S} \cdot \begin{pmatrix} x_p - t_x \\ y_p - t_y \end{pmatrix} \tag{6}$$

where (t_x, t_y, H) is the location of $\mathbf{o_i}$ in **o-xyz**, s_x and s_y are the scales related to the azimuth and range pixel sizes Δ_a and Δ_r, respectively:

$$s_x = 1/\Delta_a = 2s_a/L_e,\ s_y = 1/\Delta_r = 2s_r B/c. \tag{7}$$

Here L_e is the effective antenna aperture, B is the bandwidth of the transmitted signal, s_a is the azimuth oversampling rate related to the PRF of the system, s_r is the range oversampling rate, and c is the velocity of light. By combining (3), (5), and (6), we have

$$\begin{pmatrix} u \\ v \end{pmatrix} = \mathbf{S} \cdot \mathbf{M} \cdot \mathbf{R} \cdot \begin{pmatrix} X - T_X \\ Y - T_Y \end{pmatrix} - \begin{pmatrix} s_x t_x \\ s_y t_y \end{pmatrix}. \tag{8}$$

Equation (8) finally relates a 3D point to its projective pixel in SAR image. Under the assumption that radar moves along a track paralleling to the ground plane, the RDEs is in fact consistent with (8) because any approximation has not been used when deriving the relation, we will validate it in Section III. Nevertheless, we decompose the complex RDEs into the multiplication of three simple matrices of physical significance based on the transformations among four different coordinate systems, which helps us perform a concise and accurate SAR imaging modeling. The model involves in the system parameters s_x and s_y, the imaging geometry parameters φ, T_x, T_y, t_x, and t_y, as well as the target parameter θ. It is interesting to observe that (8)

is similar to the linear imaging model of optical camera [1] although has different meaning: here **R** as well as T_X, T_Y, $s_x t_x$, and $s_y t_y$ correspond to the transformation from the world coordinate system to the camera coordinate system by rotation and translation, **M** corresponds to the transformation from the camera system to the physical coordinate system of image by pinhole imaging, and **S** corresponds to the transformation from the image physical system to the pixel coordinate system by digital sampling. Therefore, the proposed model enables us to geometrically unify the SAR imaging and the optical camera imaging. Besides this, from (8) we can observe that the point position (X, Y) is explicitly related to the pixel position (u, v), but the point topography Z is implicit in the local incidence θ, thus the model can provide us a flexile strategy to model the SAR epipolar geometry as well as to reconstruct the target, as will be shown as follows.

B. The Rigorous Epipolar Geometry for SAR

As analyzed in Section I that the fundamental matrix and homography are inappropriate for SAR, thus in this subsection we turn to another idea to construct the SAR epipolar geometry directly from the imaging model. This kind of epipolar geometry description is less used for camera because the existing fundamental matrix and homography are both good enough, but it facilitates us to model the rigorous epipolar geometry for SAR from the developed concise imaging.

We consider a general stereoscopic configuration here. Let $\mathbf{I_1}$ and $\mathbf{I_2}$ be an image pair acquired by different SAR systems from different imaging geometries. For a 3D point (X, Y, Z) in **O-XYZ**, if its two projective pixel positions in $\mathbf{I_1}$ and $\mathbf{I_2}$ are (u_1, v_1) and (u_2, v_2), respectively, according to (8) we obtain

$$\begin{pmatrix} X \\ Y \end{pmatrix} = \mathbf{R_1^{-1}M_1^{-1}S_1^{-1}} \begin{pmatrix} u_1 \\ v_1 \end{pmatrix} + \mathbf{R_1^{-1}M_1^{-1}S_1^{-1}} \begin{pmatrix} s_{x1}t_{x1} \\ s_{y1}t_{y1} \end{pmatrix} + \begin{pmatrix} T_{X1} \\ T_{Y1} \end{pmatrix} \tag{9}$$

where the subscript 1 indexes the parameters of $\mathbf{I_1}$. Based on (8) and (9), for pixel (u_2, v_2) of $\mathbf{I_2}$ we can have

$$\begin{pmatrix} u_2 \\ v_2 \end{pmatrix} = \mathbf{S_2M_2R_2R_1^{-1}M_1^{-1}S_1^{-1}} \begin{pmatrix} u_1 \\ v_1 \end{pmatrix} + \mathbf{S_2M_2R_2R_1^{-1}M_1^{-1}S_1^{-1}} \begin{pmatrix} s_{x1}t_{x1} \\ s_{y1}t_{y1} \end{pmatrix} + \mathbf{S_2M_2R_2} \begin{pmatrix} T_{X1}-T_{X2} \\ T_{Y1}-T_{Y2} \end{pmatrix} - \begin{pmatrix} s_{x2}t_{x2} \\ s_{y2}t_{y2} \end{pmatrix} \tag{10}$$

where the subscript 2 indicates the parameters of $\mathbf{I_2}$. Therefore, by eliminating the common target position (X, Y) we can then relate the two pixels. Equation (10) can be further rearranged as

$$\begin{pmatrix} u_2 \\ v_2 \end{pmatrix} = \mathbf{A}\begin{pmatrix} u_1 \\ v_1 \end{pmatrix} + \begin{pmatrix} t_u \\ t_v \end{pmatrix} = \begin{pmatrix} s_{x1}^{-1} s_{x2} \cos\Delta\varphi & s_{y1}^{-1} s_{x2} \sin\theta_1 \sin\Delta\varphi \\ -s_{x1}^{-1} s_{y2} \sin^{-1}\theta_2 \sin\Delta\varphi & s_{y1}^{-1} s_{y2} \sin\theta_1 \sin^{-1}\theta_2 \cos\Delta\varphi \end{pmatrix} \begin{pmatrix} u_1 \\ v_1 \end{pmatrix} + \begin{pmatrix} s_{x2}\left(t_{x1}\cos\Delta\varphi + t_{y1}\sin\theta_1\sin\Delta\varphi + B_x - t_{x2}\right) \\ s_{y2}\sin^{-1}\theta_2\left(-t_{x1}\sin\Delta\varphi + t_{y1}\sin\theta_1\cos\Delta\varphi + B_y - t_{y2}\sin\theta_2\right) \end{pmatrix} \tag{11}$$

where $\mathbf{A}=\mathbf{S_2M_2R_2R_1^{-1}M_1^{-1}S_1^{-1}}$, $\Delta\varphi = \varphi_2 - \varphi_1$ denotes the rotation between the two imaging systems, and

$$\begin{pmatrix} B_x \\ B_y \end{pmatrix} = \mathbf{R_2} \cdot \begin{pmatrix} B_X \\ B_Y \end{pmatrix} \text{ with } \begin{cases} B_X = T_{X1} - T_{X2} \\ B_Y = T_{Y1} - T_{Y2} \end{cases} \tag{12}$$

where B_X and B_Y denote the initial separations between the two imaging systems in **X-** and **Y-**directions, respectively, B_x and B_y are the projections of B_X and B_Y in **x-** and **y-**directions of the second SAR imaging system, they represent the along-track and cross-track baselines, respectively. The cross-track baseline B_y is also termed as the horizontal baseline, and it refers to the baseline decorrelation which can be removed by range spectral filtering. The along-track baseline B_x is related to the temporal decorrelation of the target. The elevation, position, orientation, and scattering center of some distributed targets may change during the temporal baseline and induce a potential local translation which can be reciprocally equivalent to a baseline variance. Equation (11) is an affine transformation which models the epipolar geometry of a general SAR stereo. Interestingly, it is similar to the plane-induced homography in computer vision [1]: here $\mathbf{S_1M_1}$ and $\mathbf{S_2M_2}$ correspond to the intrinsic matrices of the two cameras, $\mathbf{R_2R_1}^{-1}$ as well as t_u and t_v correspond to the rotation and translation between the two cameras. However, different from the camera fundamental matrix and homography which are independent of the target, the SAR epipolar geometry (11) is target-dependent because the local radar incidences θ_1 and θ_2 may vary with each 3D point. This will facilitate us a much more straightforward reconstruction of the target geometry, as will be presented in Section III.

For sensors with different system parameters but the same imaging geometry, such as the multi-frequency and multi-polarization SAR systems, we have $\varphi_1 = \varphi_2$ and $\theta_1 = \theta_2$, thus (11) can be simplified as:

$$\begin{pmatrix} u_2 \\ v_2 \end{pmatrix} = \begin{pmatrix} s_{x1}^{-1} s_{x2} & 0 \\ 0 & s_{y1}^{-1} s_{y2} \end{pmatrix} \begin{pmatrix} u_1 \\ v_1 \end{pmatrix} + \begin{pmatrix} s_{x2}\left(t_{x1} - t_{x2} + B_x\right) \\ s_{y2}\left(t_{y1} - t_{y2} + B_y \sin^{-1}\theta_2\right) \end{pmatrix}. \tag{13}$$

which shows the model in this configuration is just a simple anisotropic scaling transformation.

For sensors with the same system parameters but different imaging geometries, such as the spotlight SAR, scanning SAR, and circular SAR, we have $s_{x1} = s_{x2}$ and $s_{y1} = s_{y2}$, the matrix **A** in (11) can then be written as:

$$\mathbf{A} = \begin{pmatrix} \cos\Delta\varphi & s_{y1}^{-1} s_{x1} \sin\theta_1 \sin\Delta\varphi \\ -s_{x1}^{-1} s_{y1} \sin^{-1}\theta_2 \sin\Delta\varphi & \sin\theta_1 \sin^{-1}\theta_2 \cos\Delta\varphi \end{pmatrix}. \tag{14}$$

The determinant of **A** in this case is independent of the rotation $\Delta\varphi$, which is related to the track rotation and antenna squint. The determinant involves in the area ratio of a correspondent image patch pair. Thus (14) implies that the area ratio is invariant to the track rotation and radar squint, i.e. the influence from rotation and squint may be neglected in a sense when the area ratio is considered.

If the images are further acquired from sensors of parallel tracks with the same squint, such as InSAR and radargrammetry systems, the rotation $\Delta\varphi$ in (14) can be neglected, and the epipolar geometry will then be

$$\begin{pmatrix} u_2 \\ v_2 \end{pmatrix} = \begin{pmatrix} 1 & 0 \\ 0 & \sin\theta_1 \sin^{-1}\theta_2 \end{pmatrix} \begin{pmatrix} u_1 \\ v_1 \end{pmatrix} + \begin{pmatrix} s_{x2}\left(t_{x1} - t_{x2} + B_x\right) \\ s_{y2}\left(t_{y1}\sin\theta_1 \sin^{-1}\theta_2 - t_{y2} + B_y \sin^{-1}\theta_2\right) \end{pmatrix}. \tag{15}$$

Equation (15) is an anisotropic scaling transformation, which is consistent with the existing investigations [7] [15]. It shows that the azimuth warp in this configuration is a constant translation if the along-track baseline B_x can be neglected, while the warp in range direction is related to the local target incidence of each antenna and it is target-dependent, thus the estimation of range translation is often much more difficult. We know that image registration is to compensate the geometrical warp between the images, thus (15) can be used for accurate InSAR image registration if the ground truth of the scene is available. When the image pair is acquired from gently topographic area with small baseline, the difference between θ_1 and θ_2 will be tiny, we can then empirically approximate (15) as a 2D low-order polynomial [3-5], thus (15) can direct us to determine the form and order of the polynomial. In this case we can perform the warp compensation with the algorithm such as the cross-correlation [3], and the model can then assist us to determine the correlation window size and the coherence searching scope [2].

III. 3D TARGET RECONSTRUCTION BASED ON SAR EPIPOLAR GEOMETRY

The obtained SAR epipolar geometry (11) relates the two imaged pixels (u_1, v_1) and (u_2, v_2) of a 3D point (X, Y, Z). Besides its direct application presented above, on the other hand, if the images have already been accurately aligned, the inverse application to retrieve the system parameter and target information from the matched images for system calibration and target reconstruction may be also motivated because the model also relates to the system parameter and target relief. In this section, we try to use it to retrieve the 3D information of a target from its SAR images. The radar-based target reconstruction in fact can be achieved by many techniques [16], such as the radarclinometry, radargrammetry, interferometry, and polarimetry, which use the information of shading, parallax, interferometric phase, and azimuth slope of the terrain, respectively. Here we seek to achieve it from the SAR epipolar geometry. The using of epipolar geometry of camera to retrieve the target 3D geometry has been widely carried out in the field of computer vision, where the reconstruction is usually conducted by first estimating the fundamental matrix based on point correspondences and then decompose the fundamental matrix for the camera matrix, which is just the mapping between the global 3D point and its imaged pixel [1]. This reconstruction scheme is impossible for radar since we have no fundamental matrix. However, the developed SAR epipolar geometry can enable us to achieve this more simply and straightforward because the local target incidence is included in it, thus we can directly obtain the target geometry from the constructed epipolar model.

For slant imaging, the position and elevation of a 3D point are wrapped into the imaged pixel and related to the local incidence as shown in (5) and (8). From the imaging geometry in Fig. 1 we can have

$$Z = H - R\cos\theta \tag{16}$$

where H is the platform height, Z is the target elevation, R is the slant range from APC to target, and θ is the local incidence. If radar works in the squint mode, the distance R and incidence θ should be counted from the equivalent APC. Given the pixel position (u, v), R can be easily obtained from (6) by

$$R = y_p = v/s_y + t_y. \tag{17}$$

Based on (16) we can further obtain the following constraint for the two local incidences

$$H_1 - H_2 = R_1\sqrt{1-\varepsilon_1^2} - R_2\sqrt{1-\varepsilon_2^2} \tag{18}$$

where the subscript 1 and 2 index the related parameters of the two systems, ε_1 and ε_2 respectively denote $\sin\theta_1$ and $\sin\theta_2$ so as to simplify the expression. Given the imaging parameters and pixel correspondences, the incidence retrieval can be transformed to solving either of the following two optimizations:

$$Q_1 := \min_{\varepsilon_1} \left| \begin{matrix} u_2 - s_{x1}^{-1}s_{x2}u_1\cos\Delta\varphi - s_{y1}^{-1}s_{x2}\varepsilon_1 v_1\sin\Delta\varphi \\ -s_{x2}\left(t_{x1}\cos\Delta\varphi + t_{y1}\varepsilon_1\sin\Delta\varphi + B_x - t_{x2}\right) \end{matrix} \right| \quad s.t.\ 0 \le \varepsilon_1 \le 1. \tag{19}$$

$$Q_2 := \min_{\varepsilon_1,\varepsilon_2} \left| \begin{matrix} v_2 + s_{x1}^{-1}s_{y2}\varepsilon_2^{-1}u_1\sin\Delta\varphi - s_{y1}^{-1}s_{y2}\varepsilon_1\varepsilon_2^{-1}v_1\cos\Delta\varphi \\ -s_{y2}\varepsilon_2^{-1}\left(-t_{x1}\sin\Delta\varphi + t_{y1}\varepsilon_1\cos\Delta\varphi + B_y - t_{y2}\varepsilon_2\right) \end{matrix} \right| \quad s.t. \begin{cases} H_1 - H_2 = R_1\sqrt{1-\varepsilon_1^2} - R_2\sqrt{1-\varepsilon_2^2} \\ R_1 = v_1/s_{y1} + t_{y1}, R_2 = v_2/s_{y2} + t_{y2}. \\ 0 \le \varepsilon_1 \le 1, 0 \le \varepsilon_2 \le 1 \end{cases} \tag{20}$$

Equations (19) and (20) describe two nonlinear bound-constrained optimizations. By solving either of them with the sequential quadratic programming (SQP) [17], we can then obtain the local target incidence. Based on the obtained incidence and the projective pixel positions, the 3D geometry of the target can be retrieved from (8), (16), and (17). The optimization (19) is preferred because it has only one unknown. However, for the radar stereo of negligible geometrical rotation such as that from the general InSAR and radargrammetry systems as shown in Fig. 2, the objective functions Q_1 and Q_2 will then become to

$$\begin{cases} Q_1 := \min_{\varepsilon_1} \left| u_2 - s_{x1}^{-1}s_{x2}u_1 - s_{x2}\left(t_{x1} + B_x - t_{x2}\right)\right| \\ Q_2 := \min_{\varepsilon_1,\varepsilon_2} \left| v_2 - s_{y1}^{-1}s_{y2}\varepsilon_1\varepsilon_2^{-1}v_1 - s_{y2}\varepsilon_2^{-1}\left(t_{y1}\varepsilon_1 + B_y - t_{y2}\varepsilon_2\right)\right| \end{cases}. \tag{21}$$

Q_1 in this case is independent of the local incidence, thus we can only refer to (20) for incidence estimation. The objective function Q_2 in (21) can be further expressed as:

$$Q_2 := \min_{\varepsilon_1,\varepsilon_2} s_{y2}\varepsilon_2^{-1}\left|\varepsilon_2\left(s_{y2}^{-1}v_2 + t_{y2}\right) - \varepsilon_1\left(s_{y1}^{-1}v_1 + t_{y1}\right) - B_y\right|. \tag{22}$$

By combining (17) and (22), we have

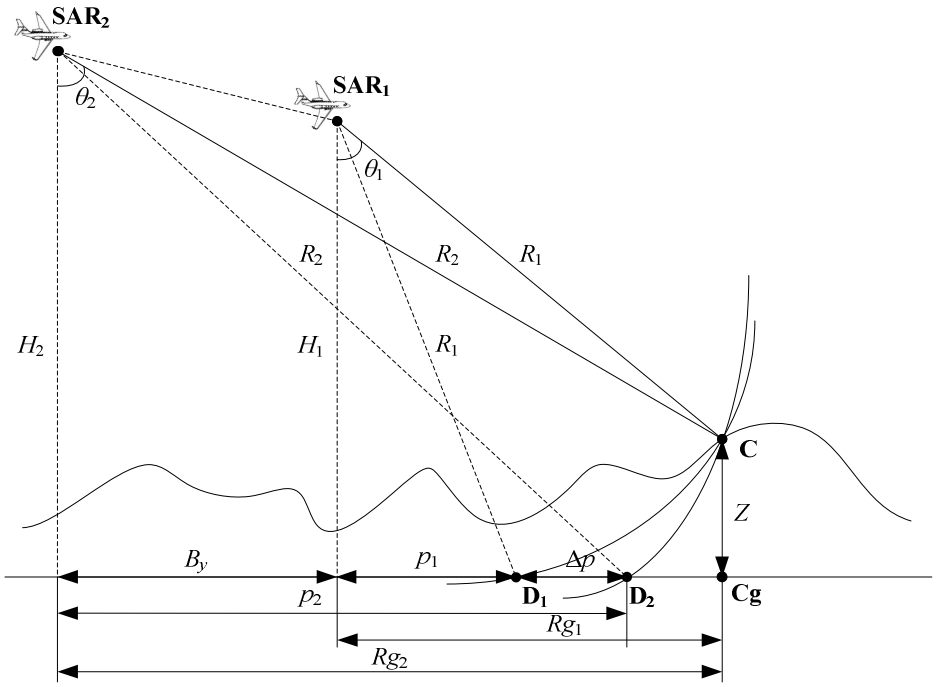

Fig. 2 The commonly-used SAR stereo configuration for interferometry or radargrammetry.

$$Q_2 := \min_{\varepsilon_1,\varepsilon_2} s_{y2}\varepsilon_2^{-1}\left|\varepsilon_2 R_2 - \varepsilon_1 R_1 - B_y\right| = s_{y2}\varepsilon_2^{-1}\left|Rg_2 - Rg_1 - B_y\right| \tag{23}$$

where R_1 and R_2 are the slant ranges from the two APCs to the target, respectively, Rg_1 and Rg_2 are the corresponding ground distances, as shown in Fig. 2. From the radar stereo we can easily obtain that

$$Rg_2 = Rg_1 + B_y \tag{24}$$

which validates (23) for elevation estimation. It is interesting to point out that in fact the radargrammetric technique also uses the similar geometrical relation as (24). The aim of radargrammetry is to extract the height information of a radar scene from a stereo pair of radar images [2] [13]. As shown in Fig. 2, the global 3D point **C** is viewed by two sensors SAR_1 and SAR_2. The obtained slant range SAR image pair is then transformed to the ground range based on the imaging geometry and registered with each other for the parallax Δp, which is the difference of ground distance between the two equidistant ground points $\mathbf{D_1}$ and $\mathbf{D_2}$ of **C** as shown in Fig. 2. The parallax Δp is related to the elevation of **C** by [2], [13]:

$$\Delta p = p_2 - p_1 - B_y = \sqrt{Rg_2^2 + \left(H_2 - Z\right)^2 - H_2^2} - \sqrt{\left(Rg_2 - B_y\right)^2 + \left(H_1 - Z\right)^2 - H_1^2} - B_y. \tag{25}$$

Therefore, the elevation can be estimated from the image parallax. Combining Fig. 2 with (23) and (25) we

TABLE I

THE IMAGING PARAMETERS OF THE SIMULATED SAR STEREO

Parameters	SAR system 1	SAR system 2
Bandwidth (B)	100 MHz	100 MHz
Antenna aperture (L_a)	1 m	1 m
Platform speed	250 m/s	250 m/s
Azimuth oversampling rate (s_a)	1.25	1.11
Range oversampling rate (s_r)	3.0	3.3
Squint angle (α)	5º	0º
Platform height (H)	5100 m	5250 m
Initial platform position in **X**-direction (T_X)	0 m	0 m
Initial platform position in **Y**-direction (T_Y)	0 m	–100 m
Rotation from **X** to flight direction (β)	0º	–7.5º
Initial pixel position in **x**-direction (t_x)	0 m	0 m
Initial pixel position in **y**-direction (t_y)	H_1/cos30º	H_2/cos25º

can see that the proposed algorithm is consistent with the radargrammetry in this case because they use the similar geometry. The only difference lies in that we perform the reconstruction directly on the slant range image pair while radargrammetry performs on the ground range images. The warp compensation on ground range images is usually much easier because the distortion from slant projection has been compensated. This may be another reason why the rigorous SAR epipolar geometry has not attracted attention so far along with the development of radargrammetry.

In the following, we test the developed imaging model, epipolar geometry, and reconstruction algorithm on a simulated SAR stereo. We consider a general stereoscopic configuration that the two SARs acquiring the image from two nonparallel tracks with different squints, as be parametrically described in Table I. Fig. 3 (a) shows some 3D target points located within the two SAR beams with X coordinate varying from 505m to 895m and Y from 3205m to 3445m, both with the sampling step of 10m. The target elevation is assumed as a saddle function of the position (X, Y) and fluctuated from 4.8m to 121m:

$$Z = 30 + 6\left(\frac{X-700}{50}\right)^2 - 3\left(\frac{Y-3350}{50}\right)^2. \tag{26}$$

In order to test the imaging model and epipolar geometry, we calculate the accurate pixel correspondence $(u_1, v_1)\leftrightarrow(u_2, v_2)$ of each target point (X, Y, Z) using the RDEs and show the results in Fig. 3 (c) and (d), respectively. We then take the first SAR pixel position (u_1, v_1) into the SAR epipolar geometry (11) for the corresponding pixel position (u'_2, v'_2) under the second SAR irradiation, and compare it with the accurate

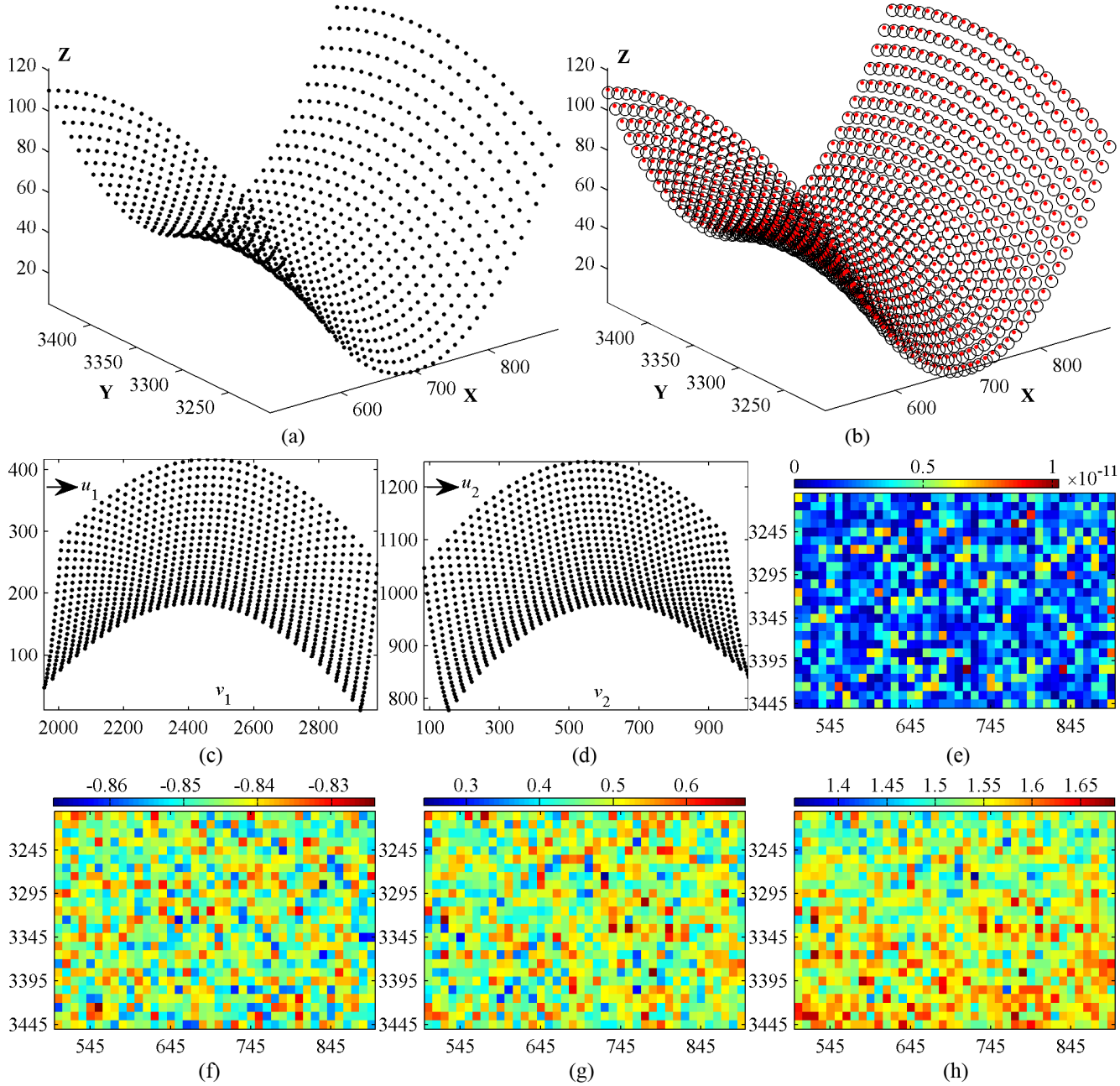

Fig. 3 (a) The real 3D target geometry and (b) its overlapping with the reconstructed one (black circle), wherein the red dot denotes the real one. The accurate projective pixel positions of the targets by (c) SAR system 1 and (d) SAR system 2 deduced from the range-Doppler equations. (e) The modeling error of each target position, which is the absolute difference between the accurate pixel position and the inversed position from the developed epipolar geometry. (f), (g), and (h) show the reconstruction errors (defined in (28)) in the directions of **X**, **Y**, and **Z**, respectively.

position (u_2, v_2) deduced by RDEs to get the modeling error (*ME*)

$$ME = |u_2 - u_2'| + |v_2 - v_2'|. \tag{27}$$

The obtained *ME* of each target position (X, Y) is shown in Fig. 3 (e), from which one can see that the error

is smaller than 10^{-10}, so the high accuracy of the epipolar geometry is validated. This can also demonstrate the consistency between the RDEs and the concise SAR imaging model because from which the epipolar geometry is directly developed.

Next we turn to reconstruct the target relief. In consideration of the reality that the extraction accuracy of the pixel correspondence can not be infinitely accurate but impacted by many factors such as the feature extraction algorithm, the inherent geometrical distortion and speckling of SAR image, here we retrieve the incidence from the artificially contaminated pixel correspondence in stead of the accurate correspondence $(u_1, v_1)\leftrightarrow(u_2, v_2)$. We conduct a Monte Carlo simulation by assuming the actual pixel position is deviated from the accurate position with an additional residue satisfying the Gaussian distribution of $G(2, 0.25)$. Based on the simulated pixel positions, by initializing the unknown ε_1 as $(R_1^2–H_1^2)^{0.5}/R_1$, we first solve (19) for incidence because the two SAR sensors work on nonparallel tracks, and then retrieve the elevation as well as the position of the target. We repeat the above simulation and reconstruction procedures 500 times, and average the 500 reconstructions of each target point for a final inversion of $(X_{inv}, Y_{inv}, Z_{inv})$. To evaluate the accuracy of the algorithm, we calculate the reconstruction error (**RE**) by

$$\mathbf{RE} = \begin{pmatrix} RE_X \\ RE_Y \\ RE_Z \end{pmatrix} = \begin{pmatrix} X - X_{inv} \\ Y - Y_{inv} \\ Z - Z_{inv} \end{pmatrix} \tag{28}$$

where RE_X, RE_Y, and RE_Z are the **RE** in each of the three directions, and they are displayed in Fig. 3 (f), (g), and (h), respectively. The results show that the maximum absolute **RE** in the three directions are 0.87m, 0.68m, and 1.69m, respectively, thus the reconstruction accuracy is around 1m. Fig. 3 (b) further shows the overlapping of the reconstructed 3D target information and the real one, from which we can see that they are perfectly overlapped with each other, so the accuracy of the algorithm is further tested.

IV. CONCLUSION

The epipolar geometry models the relation between the two pixels of a 3D point projected by a stereoscope. Since SAR acquires the image from the slant range geometry and the scene is usually of varied topography,

the widely-used descriptions of epipolar geometry developed for optical camera such as the homography and fundamental matrix are thus inappropriate for SAR. This paper is dedicated to develop a rigorous and concise modeling of the epipolar geometry for the general SAR stereo. A concise SAR imaging model is first proposed which uses a series of simple matrix transformations of clear physical significance to relate a 3D target to its imaged pixel. Based on the model, a rigorous modeling of SAR epipolar geometry is concisely obtained which can be used not only to compensate the image geometrical warp but also to inverse the imaging parameters and target relief. A SAR epipolar geometry-based target reconstruction algorithm is then proposed and shown to be consistent with radargrammetry if the special stereoscopic configuration of parallel tracks with the same squint is considered. The good performance of the developed imaging model, epipolar geometry, and target reconstruction is finally demonstrated on a simulated SAR stereo experiment. The models and algorithm are not only consistent with the existing investigations on SAR but also similar to those on camera, thus a geometrical unification of SAR imaging and optical camera imaging is attained in a sense. All these contributions should be attributed to our concise modeling of SAR imaging, which is as accurate as the RDEs under the condition that radar moves along a track paralleling to the ground plane. Although only a simulated SAR stereo is processed currently, we think the models and algorithm could be used to deal with the real SAR images particularly the high-resolution SAR images, and this is the work we are focusing on.

REFERENCES

[1] R. Hartley and A. Zisserman, *Multiple View Geometry in Computer Vision*, 2nd ed. Cambridge, U.K.: Cambridge Univ. Press, 2003, pp. 151-343.

[2] S. Meric, F. Fayard, and E. Pottier, "Radargrammetric SAR image processing," in *Geoscience and Remote Sensing*, P.-G. P. Ho, Ed. Vukovar, Croatia: In-Tech, 2009, pp.421-454.

[3] F. K. Li and R. M. Goldstein, "Studies of multibaseline spaceborne interferometric synthetic aperture radars," *IEEE Trans. Geosci. Remote Sens.*, vol. 28, no. 1, pp. 88-97, Jan. 1990.

[4] Z. Li and J. Bethel, "Image coregistration in SAR interferometry," in *Proc. Int. Arch. Photogramm., Remote Sens. Spatial Inf. Sci.*, Beijing, China, 2008, pp. 433-438.

[5] D. O. Nitti, R. F. Hanssen, A. Refice, F. Bovenga, and R. Nutricato, "Impact of DEM-assisted coregistration on high-resolution SAR interferometry," *IEEE Trans. Geosci. Remote Sens.*, vol. 49, no. 3, pp. 1127-1143, Mar. 2011.

[6] R. Abdelfattah and J. M. Nicolas, "InSAR image coregistration using the Fourier-Mellin transform," *Int. J. Remote Sens.*, vol. 26, no. 13, pp. 2865-2876, Jul. 2005.

[7] Q. Lin, J. F. Vesecky, and H. A. Zebker, "New approaches in interferometric SAR data processing," *IEEE Trans. Geosci. Remote Sens.*, vol. 30, no. 3, pp. 560-567, May 1992.

[8] A. K. Gabriel and R. M. Goldstein, "Crossed orbit interferometry: Theory and experimental results from SIR-B," *Int. J. Remote Sens.*, vol. 9, no. 5, pp. 857-872, May 1988.

[9] M. Liao, H. Lin, and Z. Zhang, "Automatic registration of InSAR data based on least-square matching and multi-step strategy," *Photogramm. Eng. Remote Sens.*, vol. 70, no. 10, pp. 1139-1144, Oct. 2004.

[10] G. Rufino, A. Moccia, and S. Esposito, "DEM generation by means of ERS tandem data," *IEEE Trans. Geosci. Remote Sens.*, vol. 36, no. 6, pp. 1905-1912, Nov. 1998.

[11] T. Toutin, "Geometric processing of remote sensing images: Models, algorithms and methods," *Int. J. Remote Sens.*, vol. 25, no. 10, pp. 1893-1924, May 2004.

[12] E. Sansosti, P. Berardino, M. Manunta, F. Serafino, and G. Fornaro, "Geometrical SAR image registration," *IEEE Trans. Geosci. Remote Sens.*, vol. 44, no. 10, pp. 2861-2870, Oct. 2006.

[13] F. W. Leberl, *Radargrammetric Image Processing*. Norwood, MA: Artech House, 1990, pp. 349-407.

[14] G. Konecny and W. Schuhr, "Reliability of radar image data," in *Proc. Int. Arch. Photogramm., Remote Sens. Spatial Inf. Sci.*, Kyoto, Japan, 1988, pp. I-92-I-101.

[15] K. Goel and N. Adam, "Three-dimensional positioning of point scatterers based on radargrammetry," *IEEE Trans. Geosci. Remote Sens.*, vol. 50, no. 6, pp. 2355-2363, Jun. 2012.

[16] T. Toutin and L. Gray, "State-of-the-art of elevation extraction from satellite SAR data," *ISPRS J. Photogramm. Remote Sens.*, vol. 55, no. 1, pp. 13-33, Feb. 2000.

[17] P. T. Boggs and J. W. Tolle, "Sequential quadratic programming," in *Acta Numerica*, A. Iserles, Ed. Cambridge, U.K.: Cambridge Univ. Press, 1995, pp. 1-51.